Available online at www.sciencedirect.com
ScienceDirect
Preprint for Applied Thermal Engineering 00 (2016) 1–19
Applied Thermal Engineering

Performance modeling and parametric study of a stratified water thermal storage tank

Aowabin Rahman[a], Amanda D. Smith[a], Nelson Fumo[b]

[a]*Department of Mechanical Engineering, University of Utah, Salt Lake City, Utah, USA, 84112*
[b]*Department of Mechanical Engineering, The University of Texas at Tyler, Tyler, Texas, USA 75799*

Abstract

Thermal energy storage (TES) can significantly increase the overall efficiency and operational flexibility of a distributed generation system. A sensible water storage tank is an attractive option for integration in building energy systems, due to its low cost and high heat capacity. As such, this paper presents a model for stratified water storage that can be used in building energy simulations and distributed generation simulations. The presented model considers a pressurized water tank with two heat exchangers supplying hot and cold water respectively, where 1-D, transient heat balance equations are used to determine the temperature profiles at a given vertical locations. The paper computationally investigates the effect of variable flow-rates inside the heat exchangers, effect of transient heat source, and buoyancy inside the tank induced by location and length of the heat exchangers. The model also considers variation in thermophysical properties and heat loss to the ambient. TES simulation results compare favorably with similar 1-D water storage tank simulations, and the buoyancy model presented agrees with COMSOL 3-D simulations. The analysis shows that when the inlet hot fluid temperature is time dependent, there is a phase lag between the stored water and the hot fluid temperature. Furthermore, it was observed that an increase in flow-rate inside the hot heat exchanger increases the stored water and the cold water outlet temperature; however, the increment in temperature observes diminishing returns with increasing flow-rate of hot fluid. It was also noted that for either heat exchanger, increasing the vertical height of the heat exchanger above a certain value does not significantly increase the cold fluid outlet temperature. Results from the model simulations can assist building designers to determine the size and configurations of a thermal storage tank suited for a given distributed generation system, as well as allowing them to accurately predict the fraction of heat generated by the system that could be stored in the tank at a given time when charging, or the fraction of heating load that could be met by the tank when discharging.

Keywords: Thermal Energy Storage, Distributed Generation, Stratified Water tank, Computational Heat Transfer, Energy Systems Modeling

NOMENCLATURE

TES	Thermal Energy Storage.
CHP	Combined Heating and Power
PGU	Power Generation Unit
CCHP	Combined Cooling Heating and Power
a	Vertical length of heat exchanger in a specific node.
A_c	Cross-sectional area of each node (m^2)

A_s Surface area of each node (m^2)

c_p Specific Heat Capacity of water (J/KgK).

d_i Inner diameter of heat exchanger (mm).

d_o Outer diameter of heat exchanger (mm).

d_{ins} Insulation thickness (mm).

D_{coil} Coil Diameter of heat exchanger (m).

f Friction factor.

F_b Body force on fluid (N).

Gr Grashof Number.

h_i Inner heat transfer coefficient (W/m^2K).

h_o Outer heat transfer coefficient (W/m^2K).

H Height of storage tank (m).

k Thermal conductivity of water (W/mK).

k_{mat} Thermal conductivity of heat exchanger material (W/mK).

k_{dest} De-stratification conductivity (W/mK).

L_{coil} Total length of heat exchanger coil (m).

m_i mass of stored water in node i (kg).

$m_{h,i}$ mass of water in hot heat exchanger in node i (kg).

$m_{c,i}$ mass of water in cold heat exchanger in node i (kg).

m_{out} mass of stored water leaving node i (kg).

m_{in} mass of stored water entering node i (kg).

N Total number of nodes

N_{coil} Number of turns in heat exchanger.

Nu Nusselt Number.

p Coil Pitch (mm).

Pr Prandtl number.

$\dot{Q_{net}}$ Net heat transferred to fluid (KW).

Ra Rayleigh Number

Re Reynolds number.

Re_{cr} Critical Reynolds number.

s Length of heat exchanger in a specific node (m).

T Stored water temperature (K).

T_h Hot water temperature (K).

T_c Cold water temperature (K).

T_i Temperature of stored water in node i (K).

$T_{h,i}$ Temperature of hot water in node i (K).

$T_{c,i}$ Temperature of cold water in node i (K).

T_{dc} Constant or steady-state component of transient temperature of inlet hot water

ΔT_{ac} Maximum amplitude of sinusoidal component of transient temperature of inlet hot water

T_∞ Ambient temperature (K).

T_s External surface temperature of storage tank cylinder (K).

$\bar{T}$ Temperature spatially averaged with respect to radial direction (K).

t time (s)

$\mathbf{u}$ Fluid velocity vector (m/s).

UA Overall heat transfer coefficient of heat exchanger (W/m^2K).

UA_{loss} Heat loss coefficient (W/m^2K).

x Vertical distance from tank water level (m).

Δx Node height (m).

δ Curvature ratio, defined as the ratio of inner tube diameter to the coil diameter ($\delta = d_i/D_{coil}$).

γ Ratio of vertical length of the heat exchanger to the node height.

μ Dynamic viscosity of water (Pa-s)

ρ Density of water (kg/m^3).

1. Introduction

Thermal energy storage (TES) can be used in conjunction with distributed energy systems for storing heat which would otherwise be wasted. A combined heating and power (CHP) system or combined cooling, heating, and power system (CCHP) recovers heat from a generation device and uses it for another useful purpose such as space or hot water heating, or absorption cooling. Generators such as engines, microturbines, and high-temperature fuel cells produce recoverable waste heat. When a CHP or CCHP system is designed to serve a specific facility, the amount of heat recovered that is used plays a significant role in the energy efficiency, profitability, and environmental friendliness of the overall system [1]. Incorporating TES can benefit the system when there are variations in temporal demand [2, 3], because the amount of recovered heat that goes toward a useful purpose is increased [4]. Additionally, TES can also provide a buffer between solar input and thermal loads for solar thermal energy collection systems.

The process works as follows: the thermal storage tank allows heat to be recovered from the power generation unit (PGU). The water that cools the PGU passes through the thermal storage tank, transferring the gained heat to the storage medium in the process. The heat gained by the thermal storage tank is then passed to the cold heat exchanger, which can then be used to meet heating loads, or passed on to an absorption chiller. A TES tank can be used as a buffer between the heat recovery step and the actual heating loads.

Water is one of the most common mediums for sensible heat TES, and the water TES tank has been studied by researchers to predict its ability to reduce energy demands and save money [5, 6, 7]. Here, a TES tank is considered as a device for heat recovery and its performance in terms of stored water temperature, outlet cold water temperature, and temperature distribution are modeled under a variety of conditions.

The stratified water TES tank is an inexpensive sensible storage medium that can be easily integrated as part of a building's energy system. Hasnain [8] suggested that due to its high heat capacity, water is well suited for low-temperature (300-375 K) applications. For a temperature differential of 60 K, water can achieve a storage density of 0.25 GJ/m^3. The water pressure in the heat exchangers and in the storage tank must be sufficiently high such that phase change of water is avoided. The sensible TES storage tank described can then be coupled with an exhaust heat recovery system for a CHP (or CCHP) application [9]. Therefore, the key cost considerations for installing such a storage tank would be the costs of insulation and construction of a high-pressure storage vessel.

The analysis method presented here provides a simple methodology describing the differential equations that govern the heat transfer taking place inside the tank, allowing for temperature predictions to be made as functions of inlet temperatures, Reynolds number, heat exchanger locations and heights, and ambient conditions. Effects of buoyancy were considered using a node-mixing model, the results from which were compared with those obtained using COMSOL simulations.

The model can be applied toward developing screening tools for the performance of an integrated TES tank during preliminary design stages for facility distributed generation systems. The screening tools are aimed at generating performance assessment results with minimal input parameters, so as to support early-stage decision making using reasonable estimates.

Most models that have been developed for similar devices consider a thermal storage tank with a single heat exchanger and net mass flow into and out of the tank. EnergyPlus [10] uses a model that can be used for a single or dual heat exchanger tank with water flowing to and from the tank directly. EnergyPlus represents the physics by deriving model equations governing the tank and heat exchanger using heat balance equations, stepping through each of the components in the thermal storage tank along with each of the heat transfer modes associated with those components. However, the software does not provide a stand-alone simulation option for thermal storage tanks.

Nakahara et al. [3] used a numerical one-dimensional model to show how stratified chilled water behaved in thermal storage tanks. The authors split the tank into two regions - in the top region, flow into the tank was considered and as such, temperature was stratified in this region, whereas the bottom piece was a fully mixed region with a uniform temperature distribution. The authors provided a method for estimating storage efficiency of a temperature-stratified water TES system and discuss its implications for designing the tank system.

A similar one-dimensional model was derived by Kleinbach et al. [11] and developed in TRNSYS to represent a residential hot water tank. Similar to the model presented here, Kleinbach's model [11] allowed for varying the number of nodes used as input to the model. Newton [12] developed a tank model in TRNSYS to incorporate internal heat exchangers, non-uniform cross-sections and net mass flow into and out of the tank. The author used several solution techniques (including Cranck-Nicholson and Euler) for solving the energy balance equation and concluded that Cranck-Nicolson method is the most accurate among the explicit solver algorithms (error $\approx 0.005\%$), while requiring only three iterations per time step.

Atabaki et al. [13] later developed a semi-empirical method dividing the tank into two regions such that the temperature distribution in one region is calculated using a quasi-one- dimensional model, while in the other region it is calculated using an experimentally-determined correlation. Their model was created to determine whether or not the mixing that occurs within a tank can be neglected, using a residential thermal storage tank with single-coil heat exchanger with flow through the tank. This study helped to conclude that the mixing effects that occur between nodes is not negligible for the system they had developed. Therefore, we investigate these effects as they pertain to our model in the initial investigation.

Other researchers have developed related models for TES integration with solar thermal systems. Buckley [14] proposed a similar model for a storage tank to be used in conjunction with a solar collector and an absorption chiller, and used an implicit finite difference scheme to solve the energy equation. Vaivudh et al. [15] proposed a model for a fully-mixed storage device to be used with a solar trough.

Angrisani et al. [5] used a 1-D model in TRNSYS to predict the temperature profile inside a stratified tank with multiple heat exchangers, and compared the model with experimental results. The 1-D model includes the effects of mass transfer within the tank, as well as mass flow into and out of the tank, thermal de-stratification and heat loss to the ambient. The model was used to validate the simplified model developed by Rahman et al. [16], who found that using 10 nodes would be adequate to accurately predict transient energy storage capacity (with less than 2% error).

The analysis presented in this paper attempts to address several limitations and research gaps in related literature. Most of the models in available literature consider a thermal storage tank where there is mass inflow and/or outflow, while the analysis presented considers a closed tank with two heat exchangers, where there is no net mass flow of stored water into or out of the tank. Aside from determining the stored water temperatures, the presented model also uses coupled heat balance equations to compute the temperature of heat transfer fluids inside the heat exchangers as functions of vertical location and time. Furthermore, while previous work has only considered free convection from heat exchanger walls to stored water as the only mode of heat transfer, the presented analysis incorporated the effect of flow-rates of heat transfer fluid exchanger by considering the contribution of forced convection inside the heat exchanger pipes. The analysis also considers the effect of varying configurations (vertical length and location) of heat exchangers on stored water and cold water temperatures.

The sections that follow describe the development of a simple, generic model that could determine the temperature profile of the fluid inside the storage tank that may be applied to various distributed energy heat recovery applications. The model also predicts the temperature profile of the heat transfer fluid in the hot and cold heat exchangers and addresses the impact of stratification on model results. The energy equations were solved using an implicit scheme,

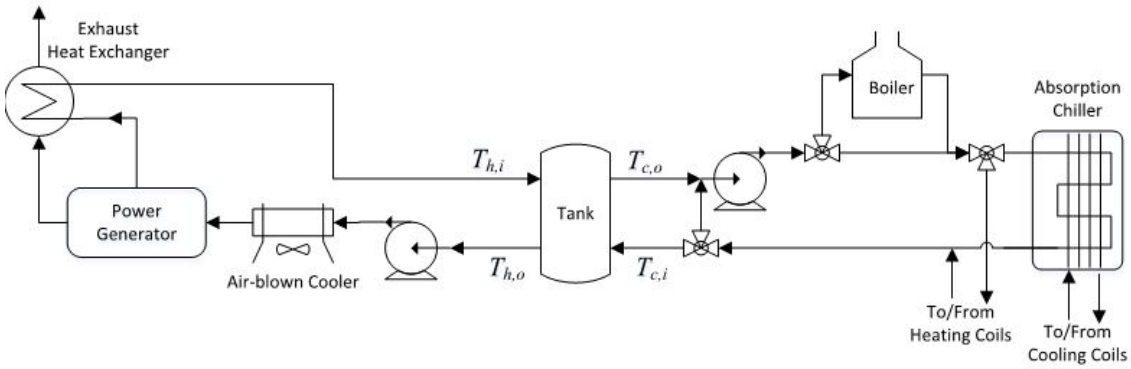

Figure 1. Schematic of a CCHP system with thermal storage

and analyzed to observe the effects of varying system parameters on water TES tank performance. The 1-D model does not capture the radial temperature gradient; however, experimental results from other literature that considered a stratified tank with flow of stored water into and out of tank showed almost negligible variation of temperature in the radial direction [2].

The main goals of this analysis are as follows:

- Develop a simple 1-D transient model of a thermal storage tank with hot and cold heat exchangers, with no flow of stored water into or out of the tank, so as to determine temperatures of stored water, as well as hot and cold water inside the heat exchangers as functions of time and vertical location.
- Conduct a parametric study on the effect of flow-rates (both within the laminar and turbulent range) and heat exchanger configurations (vertical locations of inlet and outlet ports) on the transient temperature profiles at a given vertical location.

2. Description of System

The goal of this paper is to present a mathematical model of a thermal storage that can be integrated as part of a combined cooling, heating and power (CCHP) unit (Figure 1). The power generation unit (PGU) supplies electricity to the building; however it required constant cooling for continuous operation. The coolant used to cool the PGU gains heat as it cools the PGU and from the exhaust released by the PGU. With no thermal storage integrated into the system, the heated coolant moves on to a pump that provides the heated water to an absorption chiller. A boiler is placed in parallel with the heated line in the case that more heat is necessary for the absorption chiller. This line is then returned to a pump and an air-blown cooler. The air-blown cooler is in place so that any excess heat can be dissipated before the water is provided to the PGU again for cooling. In the absence of a thermal storage, the heat being dissipated through the air-blown cooler is seen as wasted energy. With an integrated thermal storage system, a considerable fraction of thermal energy can be utilized for later use.

The thermal storage tank chosen for this analysis was one with dual heat exchangers and no flow through the tank. Therefore, the water which serves as a thermal storage medium remains in the tank, where thermal energy is added by the hot stream and is removed from the tank by the cold stream, as shown in Figure 2. For maximum heat transfer area, the heat exchanger coils run throughout the tank (although the effects of varying heat exchanger entrance and exit locations, as well as height of heat exchanger will be investigated later).

A main reason for using such a storage tank is that it allows for thermally stratified layers of water to be formed. Thermal stratification enables a high temperature layer to form at the top of the tank while creating layers descending in temperature below it until the lowest temperature layer is formed at the bottom. It has been suggested that a stratified tank could potentially be significantly more efficient at delivering thermal energy, compared to a fully-mixed

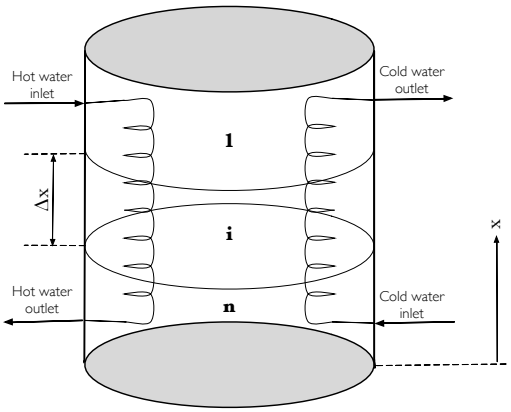

Figure 2. Schematic diagram of thermal storage model

Table 1. HEAT EXCHANGER SPECIFICATIONS [17]

Material	Stainless steel
Material Conductivity (k_{HX})	30 (W/m K)
Coil pitch (p)	36.2 mm
Coil Diameter (D_{coil})	0.49 m
Inner tube diameter (d_i)	21.6 mm
Outer tube diameter (d_o)	26.9 mm
Length of coil (L_{coil})	85.10 mm

tank of the same size [2]. The actual gain in efficiency is likely to depend on the system configuration and the load distribution over a given time interval.

The dual heat exchanger with no flow through the tank also has the advantage of being completely sealed with flow only occurring through each of the heat exchangers. This leads to less maintenance on the tank and eliminates the chance of leakage where the flow would enter and leave the tank. Additionally the dual heat exchanger arrangement enables the use of different working fluids for the supply and demand loops of the storage tank in order. The need for different working fluids arises when a single working fluid cannot meet specific requirements of the equipment in line with the loop. Figure 2 shows a simplified illustration for the one-dimensional model that will be used to develop the model.

A cylindrical thermal storage tank of diameter 1.25 m and height 2 m was considered for this analysis. Identical heat exchanger specifications, as obtained from [17] were used for both the hot and the cold heat exchangers. The specifications of the heat exchangers are give in Table 1. Using the heat exchanger specifications, the number of coils in the heat exchanger can be calculated as:

$$N_{coil} = \frac{L_{coil}}{\sqrt{(\pi D_{coil})^2 + p^2}} \tag{1}$$

3. Mathematical Model

3.1. Heat Transfer Model

The temperature profile of stored water and water in the hot and cold heat exchangers can be described by a set of 1-D transient heat transfer equations. The heat transfer equation for stored water can be expressed as:

$$m_i c_p \frac{dT_i}{dt} = \gamma UA_h(T_{h,i} - T_i) + \frac{kA_c(T_{i-1} - T_i)}{\Delta x} + \frac{kA_c(T_{i+1} - T_i)}{\Delta x} + \gamma UA_c(T_{c,i} - T_i) + UA_{loss}(T_i - T_\infty) \quad (2)$$

A new paramater γ is introduced in order to account for the variability in inlet and outlet locations of the heat exchanger (i.e. cases where the heat exchanger coils do not run throughout the entire length of the tank). As the heat exchanger and the stored water is proportional to the surface area of heat exchanger in a given node, the variability in location of heat exchanger is incorporated by multiplying the corresponding heat exchanger coefficient (UA_h or UA_c) by a factor γ, where γ is expressed as:

$$\gamma = \frac{s}{\frac{L_{coil}}{N}} = \frac{a}{\Delta x} \quad (3)$$

Here, s is the length of the heat exchanger local to a given node, L_{coil} is the total length of the heat exchanger when the entire water level of the tank is covered by the heat exchanger, a is the vertical height covered by a heat exchanger in a given node and Δx is the node length. γ is node specific for a given heat exchanger - so if stored water is fully covered in a node, $\gamma = 1$. Conversely, in nodes where the heat exchanger is absent, $\gamma = 0$.

For the heat transfer fluid (i.e. water inside the heat exchangers), the energy equations can be expressed as:

$$m_{h,i} c_{p,h} \frac{dT_{h,i}}{dt} = \dot{m}_h c_{p,h}(T_{h,i-1} - T_{h,i}) - \gamma UA_h(T_{h,i} - T_i) \quad (4)$$

$$m_{c,i} c_{p,c} \frac{dT_{c,i}}{dt} = -\dot{m}_c c_{p,c}(T_{c,i} - T_{c,i+1}) + \gamma UA_c(T_i - T_{c,i}) \quad (5)$$

The boundary values at the inlet of hot and cold heat exchangers can be incorporated as follows:

$$m_{h,1} c_{p,h} \frac{dT_{h,1}}{dt} = \dot{m}_h c_{p,h}(T_{h,in} - T_{h,1}) - UA_h(T_{h,1} - T_1) \quad (6)$$

$$m_{c,N} c_{p,c} \frac{dT_{c,N}}{dt} = -\dot{m}_c c_{p,c}(T_{c,N} - T_{c,in}) + UA_c(T_N - T_{c,N}) \quad (7)$$

The equations are subject to the following assumptions:

- There was no inflow or outflow of stored water within the tank.
- The pressure of stored water and water in the hot and cold heat exchangers are sufficiently high (0.5 MPa or higher) to prevent phase change of fluid. As such, heat transfer occurs in sensible form only.
- Temperature variation in the radial direction is negligible.
- The flow of water in the heat exchangers is fully developed.
- Due to the small thickness of the heat exchanger tubes, the transient heat capacitance of the heat exchanger walls have been neglected while calculating thermal resistances.

The heat transfer coefficients for heat transfer between stored water and water in the heat exchangers can be determined by considering the corresponding thermal resistances:

$$UA_h = \frac{1}{\frac{1}{h_{h,i}A_i} + \frac{ln\frac{d_o}{d_i}}{2\pi k_{HX}\Delta x} + \frac{1}{h_{h,o}A_o}} \quad (8)$$

$$UA_c = \frac{1}{\frac{1}{h_{c,i}A_i} + \frac{ln\frac{d_o}{d_i}}{2\pi k_{HX}\Delta x} + \frac{1}{h_{c,o}A_o}} \tag{9}$$

The heat transfer coefficient h_i can be calculated from the Nusselt number for forced, both for turbulent and laminar flow inside the heat exchangers. The heat transfer coefficient for fully-developed, turbulent flow can be expressed using the Pethukov's correlation [18]:

$$Nu_D = \frac{PrRe_D(\frac{f}{8})}{1.07 + 12.7(\frac{f}{8})^{0.5}(Pr^{0.667} - 1)} \tag{10}$$

The Pethukov correlation is valid within the Prandtl number interval $0.55 < Pr < 2000$, The Pethukov correlation for turbulent flow (eq (10)) is commonly used for straight pipes, but Castiglia et al. suggested that the correlation is valid for curved pipes as well [18]. The investigators suggested that turbulent flow in helical pipes does not significantly differ from that in straight pipes. In the case of laminar flow, counter-rotating Dean vortices are created as a consequence of centrifugal force, However, in the case of turbulent flow, turbulent perturbations break up the secondary flow developed in curved tubes, and as such, the effects of Dean vortices are minimal [18]. Castiglia et al. showed that for turbulent flow in helical pipes, the Nusselt numbers generated using the Pethukov correlation showed good parity with those obtained using CFD simulations (RMS-ω model), with RMS dispersion between 1-2% [18].

The friction factor (f) in eq (10) is determined using Ito's correlation [18]:

$$f = 0.304{Re_D}^{-0.25} + 0.029\delta^{0.5} \tag{11}$$

Ito's correlation is valid for $0.034 \leq \delta \leq 300$. The correlation for laminar flow, as suggested by Xin and Ebadian in helical pipes can be expressed as [19]:

$$Nu_D = 0.0619{Re_D}^2 Pr^{0.4}(1 + 3.455\delta) \tag{12}$$

The correlation is based on experimental results after considering multiple geometrical configurations of helical pipes and several working fluids, and is valid within the interval $5 \times 10^3 \leq Re \leq 5 \times 10^5$, $0.7 \leq Pr \leq 5$ and $0.026 \leq \delta \leq 0.088$. The critical Reynolds number for a helical pipe , which signifies transition from laminar to turbulent flow, can be expressed as [18]:

$$Re_{cr} = (2.1 \times 10^3)(1 + \delta) \tag{13}$$

Here, for $\delta = 0.04$, the critical Reynolds number $Re_{cr} = 7.39 \times 10^3$. The outer heat transfer coefficient was obtained considering free convection at the outer surfaces of the heat exchanger, and the corresponding Nusselt number was determined using correlation suggested by Ali [20]:

$$Nu_L = 0.106{Ra_L}^{0.335} \tag{14}$$

The correlation is valid within the Rayleigh number range $2 \times 10^{12} \leq Ra_L \leq 8 \times 10^{14}$, and is validated with experimental results. Ali [20] noted that in general, the Nusselt numbers calculated using equation (14) agreed well with experimental results, with a maximum deviation between the data points and the correlation obtained to be 17%. The overall heat loss coefficient can be expressed as:

$$UA_{loss} = \frac{1}{\frac{1}{2\pi k_{mat}H}\ln\frac{R_o+d_{ins}}{R_o} + \frac{1}{h_{amb}A_o}} \tag{15}$$

8

Table 2. Reference parameters for mathematical model

time step, Δt	10 s
Number of nodes, N	10
$T_{h,in}$	400 K
$T_{c,in}$	300 K
$T_{t=0}$	300 K
Re_h	1.62×10^5
Re_c	1.73×10^4

The local Nusselt number corresponding to h_{amb} was obtained using a correlation for external free convection for a thick-walled cylinder [21].

$$Nu(x)_{amb} = \left[\frac{7Gr(x){Pr_{air}}^2}{100 + 105Pr_{air}} \right]^{0.25} + \frac{4}{35} \frac{(272 + Pr_{air})}{(64 + 63Pr_{air})} \frac{x}{D_o} \tag{16}$$

$$Gr(x) = \frac{g}{\nu^2} \frac{T_s - T_\infty}{T_s + T_\infty} x^3 \tag{17}$$

This correlation for natural convection over a vertical cylinder is inclusive of all aspect ratios (L/D), as it takes into account the cases where the boundary layer thickness is comparable to the radius of curvature [21].

The differential equations (2) - (7) were solved for T_i, $T_{h,i}$ and $T_{c,i}$ using an implicit scheme in MATLAB. The computational parameters are tabulated in Table 2. The data for thermo-physical properties [22] were curve-fit to algebraic functions of temperature (in K) and as such, can be expressed as follows:

$$\mu(Pa.s) = 79.86 \exp(-0.04086T) + 0.005841 \exp(-0.008327T) \tag{18}$$

$$k(W/mK) = (-8.308 \times 10^{-6})(T^2) + 0.00656T - 0.6098 \tag{19}$$

$$c_p(J/kgK) = 0.01259T^2 - 8.035T + 5460 \tag{20}$$

$$\rho(kg/m^3) = -0.002934T^2 + 1.47T + 819.2 \tag{21}$$

As the thermo-physical properties do not vary over the time step of 10 s, the property values were lagged by one time step when solution was implemented. The root-mean-square of error in each of the equations (18) - (20) are less than 1%. The correlations are valid for pressure, $P = 0.5\ MPa$, and temperature range $273\ K \leq T \leq 420\ K$. As thermophysical properties of liquids are weak functions of pressure, the equations would be valid for higher pressures in the neighborhood of 0.5 MPa as well.

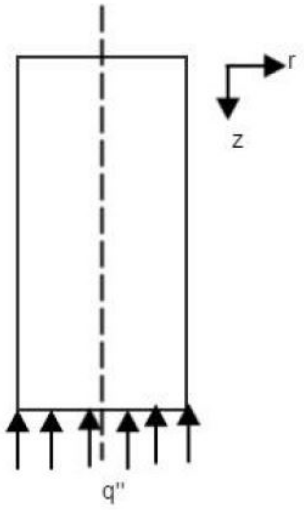

Figure 3. Schematic diagram of 2-D axisymmetric model for COMSOL simulations

3.2. Node-mixing model

The effects of buoyancy-induced mixing are incorporated using a node-mixing model. For the reference configurations (i.e location and of heat exchangers), the effects of buoyancy are minimal [16], as the corresponding temperature distribution ensures warmer fluid layers are always above colder layers. However, when the heat exchanger configurations are changed, buoyancy effects are likely to be important when the stored water temperature at the bottom layers are higher than that at the top layers. This type of unstable stratification occurs when at a given time and vertical location, the temperature gradient increases with increasing vertical distance from tank water level (i.e. $\frac{\partial T(x,t)}{\partial x} = 0$) [7]. When this happens, warmer fluid rises upwards due to buoyancy effects [12] and colder fluid moves downwards to maintain continuity. As such, the node-mixing model considers that at a given time step, when $T_{i-1} > T_i$, the fluid layers i and $i-1$ mix completely and reach a uniform temperature. This can be expressed as:

$$T_i{}^{new} = T_{i-1}{}^{new} = \frac{m_i T_i + m_{i-1} T_{i-1}}{m_i + m_{i-1}} \tag{22}$$

To investigate the accuracy of the temperature distribution obtained using the node-mixing model, the results were compared with those obtained using COMSOL simulations for a simple axisymmetric cylindrical geometry (Figure 3). The dimensions of the cylinder were considered to be identical to that of the storage tank. The bottom surface of the cylinder was assumed to be heated with a uniform heat flux of 10 KW/m^2. All other surfaces were assumed to be insulated. The boundary conditions for the COMSOL simulation were:

$$\frac{\partial T(r=r_o,x,t)}{\partial r} = \frac{\partial T(r,x=0,t)}{\partial x} = 0$$

$$\frac{\partial T(r=0,x,t)}{\partial r} = 0$$

$$q''(r, x = H, t) = 10\ KW/m^2$$

COMSOL Multiphysics uses continuity, momentum and energy balance equations for single phase, incompressible flow in order to find the temperature at each (r,z) location. The equations can be expressed as:

$$\rho \nabla.(\mathbf{u}) = 0 \tag{23}$$

$$\rho\frac{\partial \mathbf{u}}{\partial t} + \rho(\mathbf{u}.\nabla)\mathbf{u} = -\nabla P + \mu(\nabla\mathbf{u} + \nabla\mathbf{u}^T) + F_b \tag{24}$$

$$\rho c_p\frac{\partial T}{\partial t} + \rho(\mathbf{u}.\nabla T) - \nabla(k\nabla T) = \dot{Q_{net}} \tag{25}$$

The equations (23) - (25) are integrated as part of COMSOL package and the problem is set up as detailed in the COMSOL manual [23]. It should be noted that the buoyancy model in COMSOL is only being used as a validation tool for the 1-D transient model presented in this paper. Validations of the buoyancy model in COMSOL with respect to experimental results have been shown by Nowak et al. for heating inside an enclosed vertical cylinder [24].

To reduce the dimension of the temperature distribution obtained in COMSOL so as to compare it with the 1-D transient model with node-mixing, the temperature at a given vertical location was spatially-averaged with respect to the radial direction:

$$\bar{T}(x,t) = \frac{\int_0^{r_o} T(r,x,t)\,(2\pi)\mathrm{d}r.}{\pi {r_0}^2} \tag{26}$$

The root-mean-square (RMS) of the difference in temperatures obtained using the 1-D transient model with node-mixing and the COMSOL simulation over a time period of 1800 seconds is 1.01 K. The difference in temperature is highest near the heated boundary, where the node-mixing model under-predicts the local node temperature.

4. Results and Discussion

4.1. Thermal storage behavior under constant and transient inlet hot water temperatures

Figures 4-6 describe how stored water, hot water and cold water temperatures vary when the inlet hot water temperature is constant). Figure 4 shows the transient temperature profiles of stored water at x/H = 0.05, 0.55 and 0.95 respectively with reference configurations (Table 2), as obtained considering a 10-node. Previous work [16] has established that considering an excess of 10 nodes does not significantly improve the accuracy. Additionally, models with an excessive number of nodes might predict stratification that is difficult to achieve in practice [11]. The plot shows that for the given configuration, the local temperature profiles appear to be reaching steady-values at about 3-hour mark. The plot also shows that for the given configurations, the steady-state temperature at the bottom node is almost twice of that at the top node.

Figures 5 and 6 present the corresponding temperature profiles of water in the hot and cold heat exchangers respectively, as obtained from the coupled partial differential equations. The temperature in the plots are presented in terms of dimensionless temperatures T^*, ${T_h}^*$ and ${T_c}^*$, which are defined as follows:

$$T^* = \frac{T - T_{t=0}}{T_{h,in} - T_{c,in}} \tag{27}$$

$${T_h}^* = \frac{T_h - T_{h,t=0}}{T_{h,in} - T_{c,in}} \tag{28}$$

$${T_c}^* = \frac{T_c - T_{c,t=0}}{T_{h,in} - T_{c,in}} \tag{29}$$

The temperature differences are normalized with respect to the difference in temperature of inlet hot water $T_{h,in}$ and that of inlet cold water $T_{c.in}$. Figures 5 and 6 show that hot-water and cold-water temperatures also reach steady-state at around the 3-hour mark. With the heat exchanger operating in counter-flow mode, the outlet temperature of hot water is the local temperature at the bottom node (i.e.${T_h}^*(x/H = 0.95)$), whereas that for the cold water is ${T_c}^*(x/H = 0.05)$. Figure 6 also shows that for the reference parameters considered (table 2), the gain in cold water temperature at outlet is about 60% of the temperature difference between the hot and cold water.

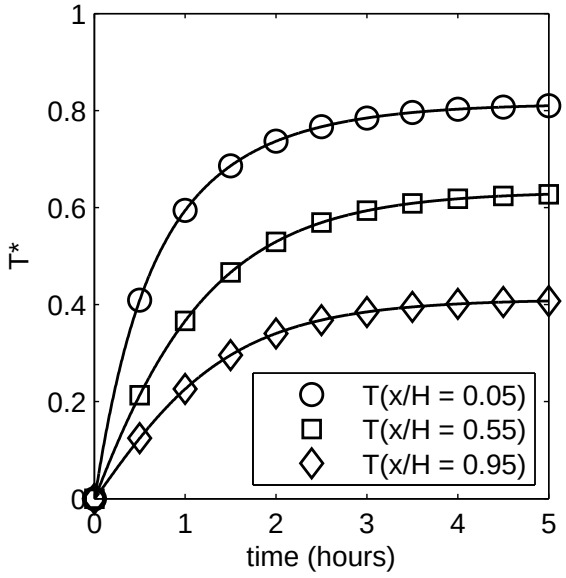

Figure 4. Temperature profile of stored water at x/H = 0.05, 0.55 and 0.95

However, the behavior of distributed energy systems is often time-dependent [25], and as such, there is a need to analyze the response of a thermal storage, in terms of phase/time lag, when the inlet hot water temperature is transient. A common approach to simulate the transience of heat source is to use a sinusoidal function [26], and as such, the input hot water temperature can be decomposed into a constant (or a "dc") and a sinusoidal (or an "ac" component):

$$T_{h,in}(t) = T_{dc} + \Delta T_{ac} sin(2\pi\omega t) \tag{30}$$

The transient inlet temperature can be non-dimensionalised as:

$$T_{h,in}(t)^* = \frac{T_{h,in}(t) - T_{h,t=0}}{T_{h,in,max} - T_{c,in}} \tag{31}$$

Here, $T_{h,in,max}$ is the maximum possible temperature of inlet hot water. Considering a sinusoidal perturbation such that T_{dc} = 387.5 K, ΔT_{ac} = 12.5 K and $T_{h,in,max}$ = 400 K, $T_{h,in}(t)^*$ can be expressed as:

$$T_{h,in}(t)^* = 0.875 + 0.125 sin(2\pi\omega t) \tag{32}$$

Here, $\omega = 1/1800$, where the time period associated with the transience in inlet temperature is 1800 seconds.

Figures 7 through 9 show how the stored water varies due to the effect of the transient heat source. Figure 7 shows that as vertical distance from the top of the tank increases, the fluctuations in stored water temperature decrease. However, the temperature fluctuations in each vertical location are in phase with each other. Due to the thermal capacitance of stored water mass inside the tank, there is a time lag between the hot water temperature and the stored water temperatures. The time lag is equal to 0.15 hours or a phase lag of 1.88 radians. Figure 8 illustrates that the average stored water temperature and the cold water temperature are in phase (i.e. both have an identical phase lag with respect to inlet hot water). This is due to the fact that the thermal capacitance of the cold water in the heat exchanger is fairly small compared to the thermal capacitance of stored water in the tank ($\frac{\dot{m}_c c_{p,c} t_p}{m c_p} \approx 0.05$).

Figure 9 shows how the demand response of cold outlet water varies with its Reynolds number. Expectedly, the temperature (both the steady-state and the fluctuation component) of cold water decrease with increasing cold water flow rate. The plot also shows that there is an almost negligible change in phase lag while increasing the flow-rate from $Re_c = 2.16 \times 10^3$ to $Re_c = 6.48 \times 10^4$ — indicating that increasing the flow-rate would not reduce the time delay of outlet cold water.

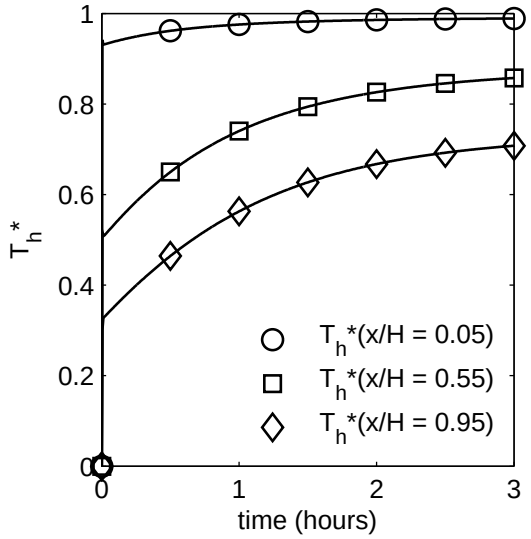

Figure 5. Temperature profile of water in the hot heat exchanger

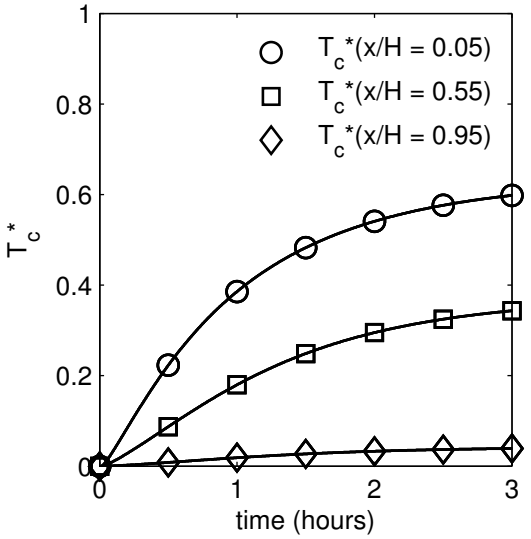

Figure 6. Temperature profile of water in the cold heat exchanger

4.2. Effect of flow-rates in the heat exchangers

Figure 10 shows the steady-state temperature distribution of stored water under variable flow-rates of hot water, while Figure 11 shows the corresponding effect on outlet cold water temperature. The Reynolds numbers corresponding to the flow-rates are in the interval $Re_h = [2.17 \times 10^3, 2.43 \times 10^5]$. $Re_h = 2.17 \times 10^3$ corresponds to laminar flow, as $Re_h < Re_{cr}$. Figure 10 shows that the degree of stratification within the tank decreases with increasing flow-rate of hot water. With increasing flow-rate (and thereby increasing Re_h), the magnitude of heat transferred increases and as such, by the time steady-state is reached, the temperature of the bottom nodes increase.

The plot also shows that above $Re_h = 1.62 \times 10^5$, there is very little gain in temperature of outlet cold water. For internal forced convection, the corresponding Nusselt number increases with increasing Reynolds number [27], which increases overall heat transfer coefficient (UA_h). However, the heat transfer is constrained by the temperature difference between the inlet hot water and the temperature of stored water in the tank. As the bottom nodes get heated, the average temperature of stored water increases, which reduces the heat transfer rate over time.

Figure 12 similarly shows the steady-state temperature distribution of stored for varying turbulent cold water flow-rates within the Reynolds number interval $Re_h = [2.17 \times 10^3, 2.43 \times 10^5]$, while maintaining a constant hot water flow-rate at $Re_h = 1.82 \times 10^5$. The degree of stratification is observed to decrease with increasing flow-rate of cold water. As the heat exchangers are in counter-flow arrangement, the heat transfer between the cold water and stored water primarily occurs at the bottom nodes for relatively lower flow-rates (and thereby lower Re_c); however, with increasing flow rate, the magnitude of heat transferred between the cold water and stored water at the top nodes increases. This results in a drop in temperature at the top nodes with increasing flow-rate. Figure 13 shows that while the cold-water temperature decreases with increasing flow-rate, beyond $Re_c = 4.32 \times 10^4$, there is diminishing returns with regards to decrements in cold water temperature. Once again, this is due to the fact that the heat transfer rate is limited by the inlet temperature of cold water.

Figure 14 shows how the heat transfer rate varies with time for different flow-rates of hot water, over a time interval of 3 hours. For low Re_h, the magnitude of heat transferred (Q_h) almost remains constant over the 3-hour period. As it has been established in Figure 10, for low Re_h, Q_h is sufficiently low, so the stored-water temperature at the bottom nodes do not increase significantly over the three-hour mark. As such, at low Re_h, the hot water could still "access" the bottom nodes. For higher flow-rates, the temperature of bottom nodes increase with time, and as such, Q_h decreases. Figure 15 plots Q_h at the end of three-hour period as a function of hot water Reynolds number Re_h and re-iterates that at high flow-rates, there is diminishing gain in Q_h with respect to Re_h.

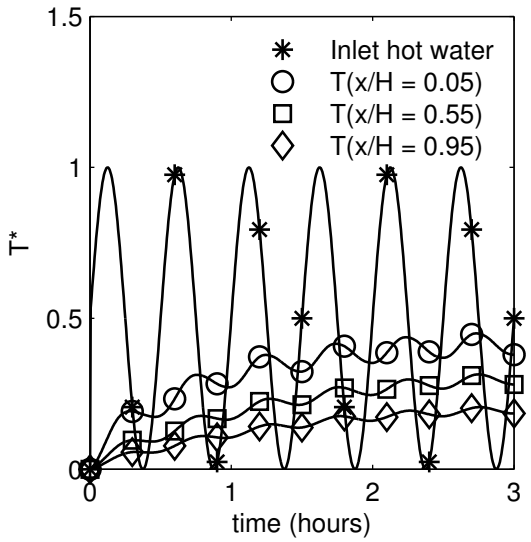

Figure 7. Temperature profile of stored water under transient heating

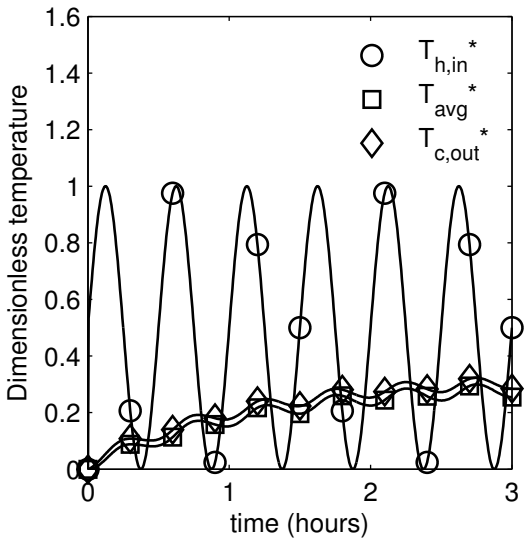

Figure 8. Temperature profile of inlet hot water, average stored water and outlet cold water under transient heating

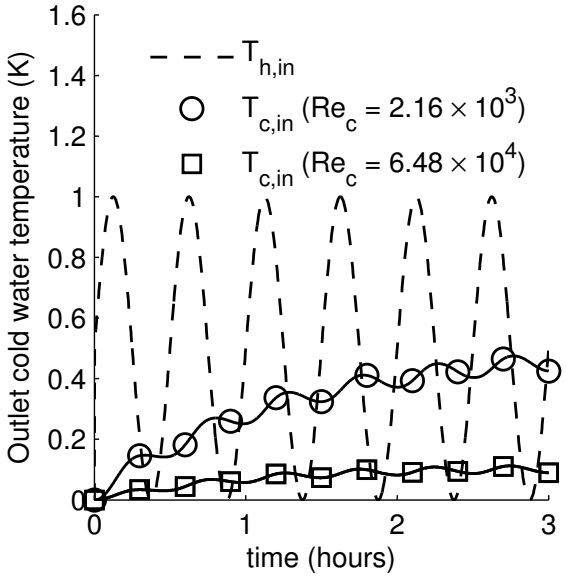

Figure 9. Temperature profile of cold water under transient heating at different cold water Reynolds numbers

4.3. Heat exchanger length and location

Next, the effects of changing the location and length of the heat exchangers on the steady-state temperature distribution and the cold water temperature outlet were investigated. Figures 16 - 19 show the effect of varying heat exchanger locations. The notation $[x_1, x_2]$ is used to represent a heat exchanger whose vertical location of inlet is x_1 and the vertical location of outlet is x_2.

To start with, the inlet and outlet locations of the cold heat exchanger is varied, while keeping the inlet and outlet locations of hot heat exchanger constant at [0, 2]. Figure 16 presents the steady-state temperature distributions for different locations of the cold heat exchanger, when the vertical length of the hot and cold heat exchangers were kept constant at 2 m and 1 m, respectively. Figure 16 shows that when the cold heat exchanger is moved up vertically

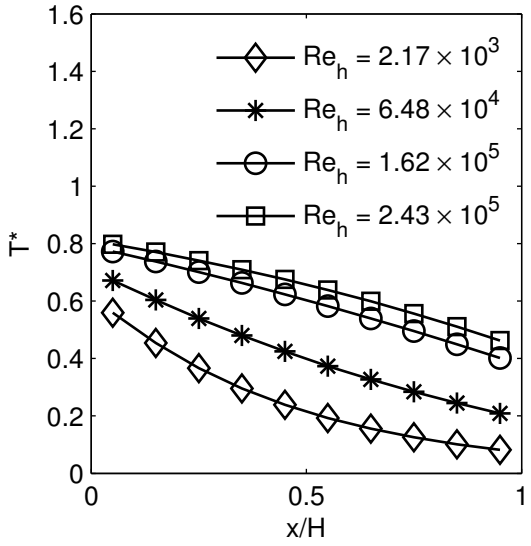

Figure 10. Steady-state temperature distribution under different hot water Reynolds number

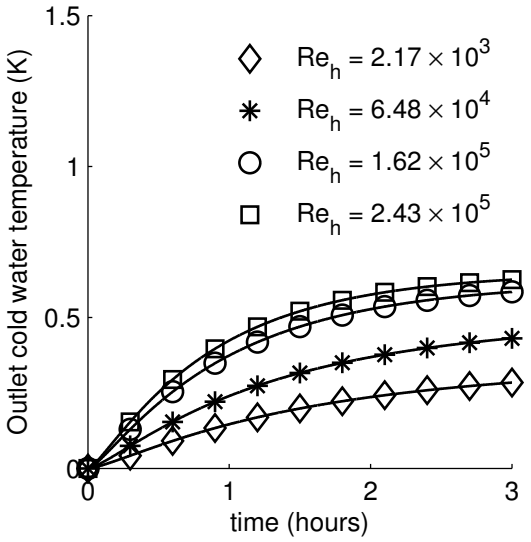

Figure 11. Cold water outlet temperature under different hot water Reynolds number

within the storage tank, the degree of stratification within the tank decreases. This occurs when the inlet and outlet locations of cold water are shifted higher up the storage tank. The local stored water temperature, where the stored water is in thermal contact with the cold water in the heat exchanger, momentarily becomes lower than the stored water temperature in lower nodes, creating unstable stratification. Thus, when $T_i < T_{i+1}$, buoyancy-induced mixing occurs between the nodes until a uniform temperature is reached. As such, when the cold heat exchanger is located higher up the tank (as is the case with [1.10, 0.10] configuration), a flatter temperature profile is observed.

Figure 17 presents the corresponding cold water outlet temperature profiles as a function of time. It can be observed that that over a 3-hour period, the cold water outlet temperature is higher when the inlet and outlet locations of the cold heat exchanger are shifted upward. This is due to the stratification within the tank, so when the cold heat exchanger is located higher up the tank, the cold water reaches the warmer stored water in the top nodes.

Figure 18 illustrates the effect of changing inlet and outlet locations of the hot heat exchanger, while maintaining the vertical length of the hot and cold heat exchangers constant at 1 m and 2 m respectively. As the hot heat exchanger is shifted downward, buoyancy effects become more significant, reducing stratification within the tank.

Figure 19 illustrates that varying the location of hot heat exchanger does not have a significant influence on the cold water outlet temperature. It should be noted that the results in figure 19 are obtained for a 1-D assumption. If the radial variation in temperature was considered, it would have likely that the cold water outlet temperature would have been higher for cold heat exchangers located at the top compared to those located at the bottom, due to the stratification of stored water temperature within the tank. However, the effect of radial temperature gradient is likely to be small [2].

Figures (20) - (22) demonstrate the effect of varying height of heat exchanger on the steady-state temperature distribution of stored water and the cold water outlet temperature profiles. Figure 20 shows the temperature distribution in the tank when the vertical length of the cold heat exchanger is varied while keeping the location of heat exchanger outlet constant (x_2 = 0.1 m). The degree of stratification expectedly increases with the vertical height of the cold heat exchanger, as the bottom nodes are cooled when the inlet cold heat exchanger is located further down the tank. Similarly, Figure 21 similarly shows the effect of changing the vertical height of the hot heat exchanger, while keeping the inlet location constant (x_1 = 0.1 m). The local stored water temperature predictably drops at outlet hot water locations.

Figure 22 shows the effect of changing the vertical length of both the hot and cold heat exchangers on the outlet temperature of cold water at steady-state (i.e. outlet temperature of cold water at the 3-hour mark). When the vertical length (h_{HX}) of the hot heat exchanger was varied, the vertical length of the cold heat exchanger was kept constant at

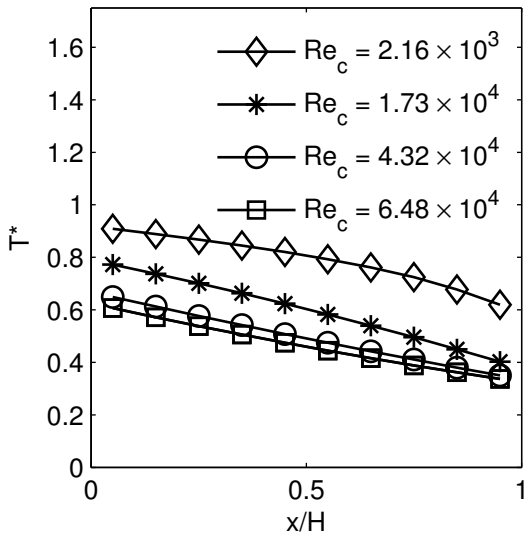

Figure 12. Steady-state temperature distribution under different cold water Reynolds number

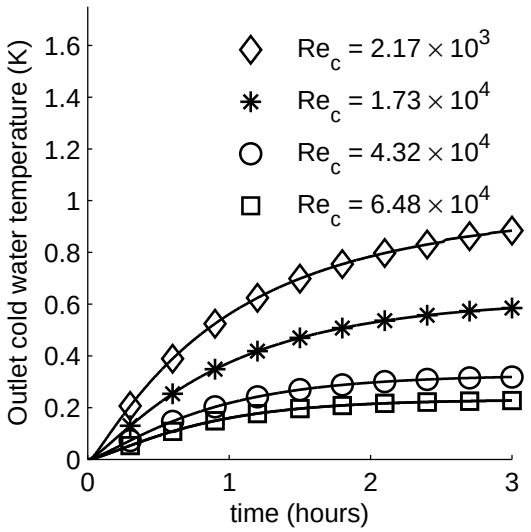

Figure 13. Cold water outlet temperature under different cold water Reynold's number

2 m (and vice versa).

When a parametric study was conducted to investigate the effect of vertical length of cold heat exchanger, the outlet location of cold heat exchanger was kept constant at (x_2 = 0.1 m). In other words, the inlet/outlet locations for hot and cold heat exchangers were $[0, 2]$ and $[h_{HX}/H + 0.1, 0.1]$ respectively. Figure 22 shows that for the aforementioned heat exchanger configurations, there are diminishing returns with increasing height of cold heat exchanger. Because of the stratification within the tank, there is reduced heat transfer at the bottom nodes compared to the top nodes. Thus, with the outlet constant at top node and with increasing height of cold heat exchanger, the incremental change in cold water outlet temperature starts to diminish as the height of the cold heat exchanger increases.

Subsequently, a parametric study was conducted to observe the effect of vertical length of hot heat exchanger, in which case the inlet location of the hot heat exchanger was maintained at 0.1 m. As such, the corresponding configurations for hot and cold heat exchanger were $[0.1, h_{HX}/H + 0.1]$ and $[2, 0]$. Figure 22 shows that there are some diminishing returns with increasing height of hot heat exchanger as well. The hot water is cooled as it flows down, and so the local heat transfer rate is lower at the bottom nodes compared to the top. As a result, the incremental change in cold water outlet temperature also diminishes as the height of the hot heat exchanger increases.

4.4. Heat loss to ambient

For the given configurations, the heat loss coefficient UA was calculated to have a constant value of 0.2026 W/K over the time period of 3 hours for an insulation thickness of 200 mm. As UA_{loss} does not vary for the given insulation thickness and ambient temperature (300 K), iterative computation of UA at each time step can be avoided. This can be explained by considering the ratio $\frac{UA_{loss}}{\dot{m}_h c p_h}$, which is in the order of 10^{-5}. For the given thermal storage tank, heat is being continuously supplied and retrieved from the stored water. As such, the magnitude of heat transfer from the heat transfer fluids (i.e. hot and cold water) and stored water are significantly higher than the magnitude of heat lost to ambient.

Figure 23 shows how the heat transfer coefficient at steady-state varies with insulation thickness. The heat transfer coefficient decreases over the range of insulation thickness between 0.5 mm and 500 mm. The critical insulation thickness for this tank is below 0.1 mm. The plot also shows that above an insulation thickness of 200 mm, the decrease in UA_{loss} starts to diminish significantly. As the material cost increases with increasing thickness of insulation, an insulation of 200 mm was considered for this storage tank.

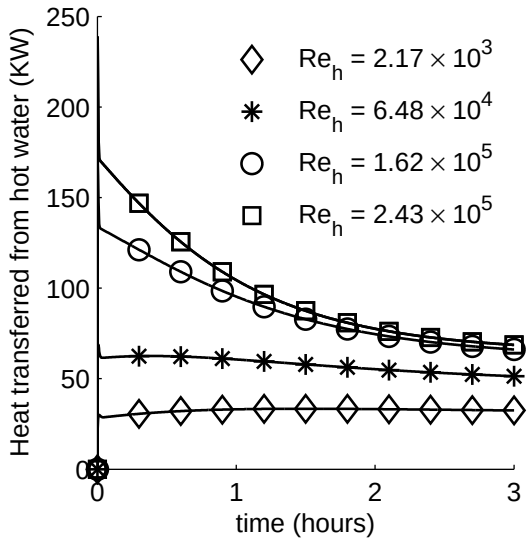

Figure 14. Heat transfer rate under different hot water Reynold's number

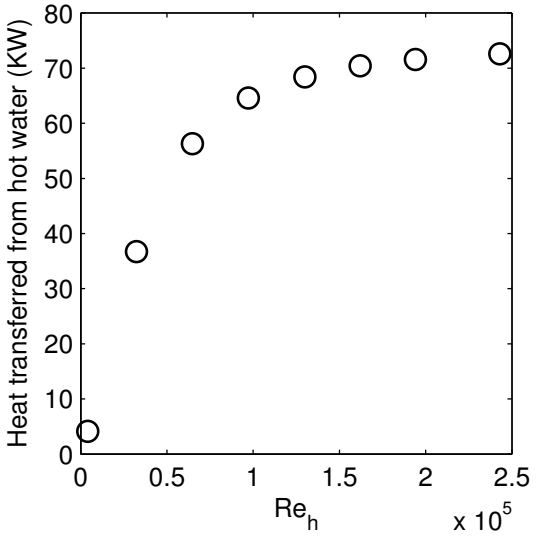

Figure 15. Cold water outlet temperature under different hot water Reynold's number

5. Conclusions

In summary, this analysis was conducted as follows:

- A simple 1-D transient model of a thermal storage tank was developed using a 10-node model accounting for heat transfer and a node-mixing model to represent buoyancy within the tank. The device contains hot and cold heat exchangers, with no flow of stored water into or out of the tank, and predicts hot heat exchanger, cold heat exchanger, and stored water temperatures as functions of time.
- A parametric study was performed on the effect of flow rates and heat exchanger configurations on the transient temperature profiles at a given vertical location.

The counter-flow arrangement of the heat exchangers and buoyancy effects cause stratification of temperature within the tank. The degree of stratification was observed to depend on the relative Reynold's numbers of heat transfer fluids in the hot and cold heat exchangers, as well as the relative location and height of the heat exchangers. When the inlet temperature is perturbed using a sinusoidal function, it was observed that the thermal capacitance of the stored water mass causes the temperature of stored water to lag behind that of hot water, while the cold water at outlet remains in phase with the stored water irrespective of its Reynold's number. Such results could potentially be useful in applications where the heat exchanger is integrated with a transient heat source (e.g. exhaust gas of an IC engine or a solar collector).

The results also show that for a given cold water Reynold's number (Re_c), the gain in cold water temperature diminishes with increasing hot water Reynold's number (Re_h). Similarly, the decrement in cold water temperature corresponding to increasing Re_c (and constant Re_h) also observes diminishing returns. This is due to the fact that the heat transfer between stored water and heat transfer fluid is limited by the temperature difference between the inlet hot water and inlet cold water.

For a given height, entrance and exit locations of heat exchangers that promote buoyancy-induced mixing was observed to reduce stratification in the tank, and the cold water outlet temperature increases when the cold heat exchanger is located at the top. Increasing height of either hot and cold heat exchanger was observed to increase the outlet cold water temperature, although beyond a height of $h_{HX}/H = 0.75$, the gain in temperature is small.The computations also show that for such a thermal storage system where heat is being supplied continuously, the effects of heat loss to ambient can be ignored.

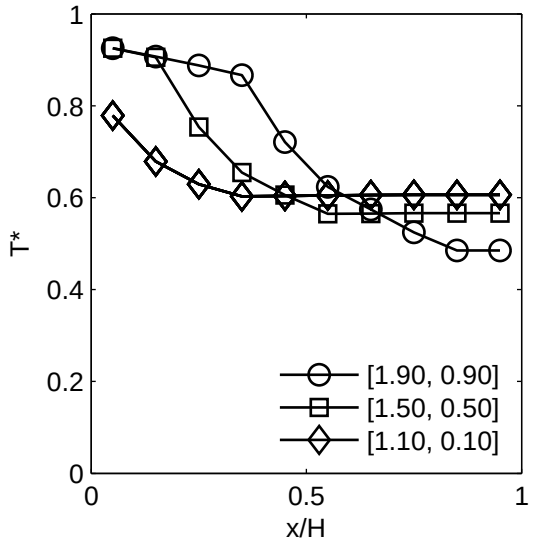

Figure 16. Steady-state temperature distribution for different locations of cold heat exchanger. The height of the hot heat exchanger kept constant at 2 m.

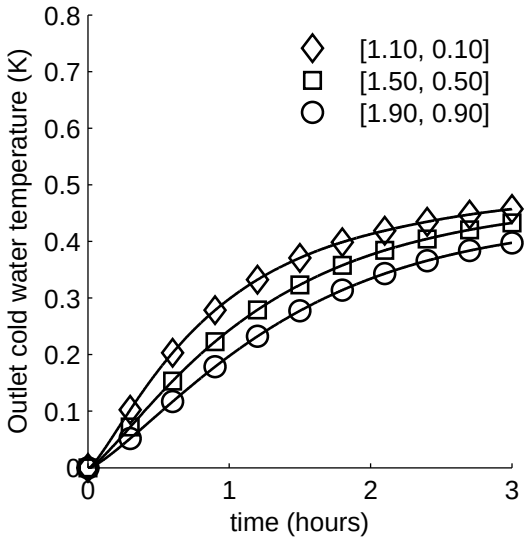

Figure 17. Cold water outlet temperature for different locations of hot heat exchanger. The height of the cold heat exchanger kept constant at 2 m.

References

[1] P. J. Mago, A. D. Smith, Evaluation of the potential emissions reductions from the use of CHP systems in different commercial buildings, Building and Environment 53 (2012) 74–82.
[2] C. A. Cruickshank, Evulation of a Stratified Multi-Tank Thermal Storage for Solar Heating Applications, Ph.D. thesis, Queen's Unviersity, Kingston, Ontario, Canada (2009).
[3] N. Nakahara, K. Sagara, M. Tsujimoto, Water thermal storage tank: Part 2-mixing model and storage estimation for temperature-stratified tanks, ASHRAE Transactions 95 (2) (1989) 371–394.
[4] A. D. Smith, P. J. Mago, N. Fumo, Benefits of thermal energy storage option combined with CHP system for different commercial building types, Sustainable Energy Technologies and Assessments 1 (2013) 3–12.
[5] G. Angrisani, M. Canelli, C. Roselli, M. Sasso, Calibration and validation of a thermal energy storage model: Influence on simulation results, Applied Thermal Engineering 67 (2) (2014) 190–200.
[6] N. DeForest, G. Mendes, M. Stadler, W. Feng, J. Lai, C. Marnay, Optimal deployment of thermal energy storage under diverse economic and climate conditions, Applied Energy 119 (2014) 488–496.
[7] Y. M. Han, R. Z. Wang, Y. J. Dai, Thermal stratification within the water tank, Renewable and Sustainable Energy Reviews 13 (5) (2009) 1014–1026.
[8] S. Hasnain, Review on sustainable thermal energy storage technologies, Energy Conversion and Management 39 (2) (1998) 1127–1138.
[9] A. Celador, M. Oriozola, J. Sala, Implications of the modelling of stratified hot water storage tanks in the simulation of chp plants, Energy Conversion and Management 52 (2011) 3018–3026.
[10] National Renewable Energy Laboratory (U.S.), EnergyPlus Documentation (2015).
[11] E. Kleinbach, W. Beckman, S. Klein, Performance study of one dimensional models for stratified thermal storage tanks. solar energy, Solar Energy 50 (2) (1993) 155–166.
[12] B. Newton, Modeling of solar storage tanks, Master's thesis, University of Wisconsin, Madison (1995).
[13] N. Atabaki, M. Bernier, Q semi-emperical model for residential electric hot water tanks, ASHRAE Transactions 111 (1) (2005) 159–168.
[14] R. C. Buckley, Development of an Energy Storage Tank Model, Ph.D. thesis, University of Tennessee at Chattanooga (2012).
[15] V. Vaivudh, W. Rakwichian, S. Chindaruksa, Heat transfer of high thermal energy storage with heat exchanger for solar trough power plant, Energy Conversion and Management 49 (11) (2008) 3311–3317.
[16] A. Rahman, A. D. Smith, N. F. Fumo, Simplified modeling of thermal storage tank for distributed energy heat recovery applications, in: ASME 2015 Power and Energy Conversion Conference, American Society of Mechanical Engineers, 2015.
[17] W. Logie, E. Frank, M. Rommel, Investigation of immersed coil heat exchangers in regard to heat transfer and storage stratification, in: EuroSun, 2010, pp. 1–10.
[18] F. Castiglia, P. Chiovaro, M. Ciofalo, M. D. Liberto, P. Maio, I. D. Piazza, M. Giardina, F. Mascari, G. Morana, G. Vella, Modelling flow and heat transfer in helically coiled pipes . part 3: Assessment of turbulence models , parametrical study and proposed correlations for fully turbulent flow in the case of zero pitch, Tech. rep., Agenzia Nazionale per le Nuove Tecnologie l'Energie e lo Sviluppo Economico Sostenibile (2010).
[19] L. Cattani, Numerical investigation of the convective heat transfer enhancement in coiled tubes, in: 2012 COMSOL Conference in Milan, 2012.

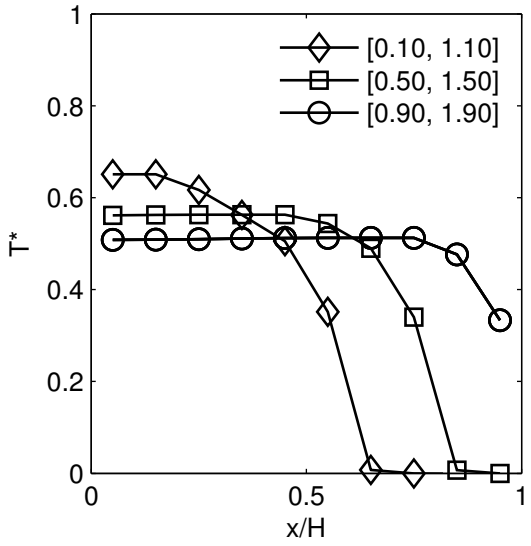

Figure 18. Steady-state temperature distribution for different locations of cold heat exchanger. The height of the hot heat exchanger kept constant at 2 m.

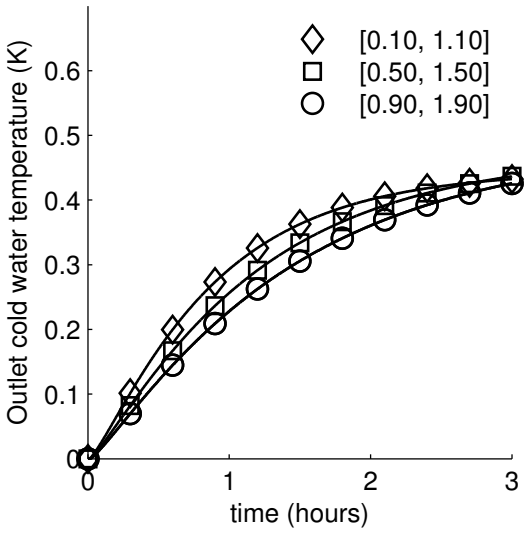

Figure 19. Cold water outlet temperature for different locations of hot heat exchanger. The height of the cold heat exchanger kept constant at 2 m.

[20] M. Ali, Free convection heat transfer from the outer surface of vertically oriented helical coils in glycerol-water solution 40 (8) (2003) 615–620.

[21] E. Le Fevre, Laminar free convection from a vertical plane surface, in: Proceedings of the 9th International Congress of Applied Mechanics, Brussels, Vol. 4, 1956, pp. 168–174.

[22] Fluids property calculator.
URL `https://www.irc.wisc.edu/properties/`

[23] COMSOL Multiphysics 5.0, Solved with COMSOL Multiphysics 5.0 - Buoyancy Flow in Water.

[24] E. S. Konrad Nowak, Marek Markowski, Modeling the natural convection heating of liquid in a vertical cylinder, Techn. Sc. (13) (2010) 11–21.

[25] D. Haeseldoncx, L. Peeters, L. Helse, W. D'haeseleer, The impact of thermal storage on the operational behavior of residential chp facilities and the overall co2 emissions, Renewable and Sustainable Energy Reviews 11 (2007) 1227–1243.

[26] C. R. Tugores, H. Francke, F. Cudok, A. Inderfurth, S. Kranz, C. Nystech-Geusen, Coupled Modeling of a District Heating System with Aquifer Thermal Energy Storage and Absorption Heat Transformer, in: International Modelica Conference, 2015, pp. 195–206.

[27] K. Saravanan, An experimental investigation of heat transfer coefficients of spiral plate heat exchanger, Modern Applied Science 5 (2) (2008) 14–20.

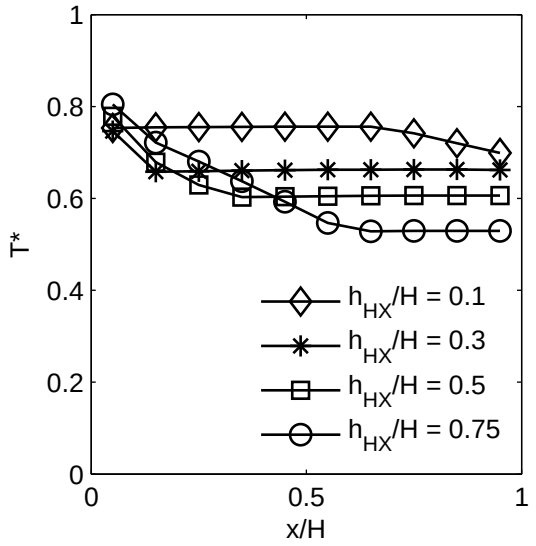

Figure 20. Steady-state temperature distribution for different height of cold heat exchanger. Height of hot heat exchanger maintained at 2 m and exit location of cold water maintained at $x_2 = 0.1\ m$

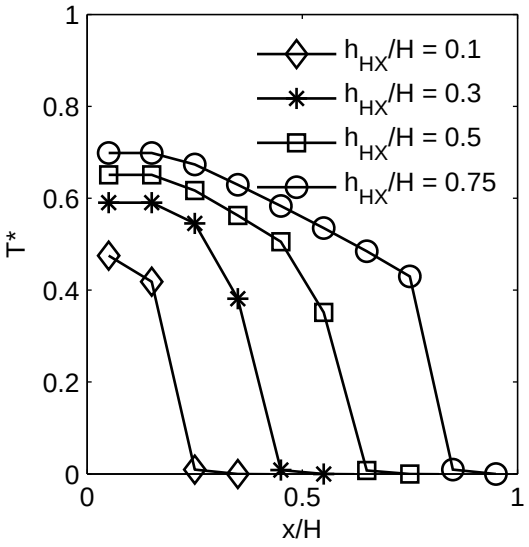

Figure 21. Steady-state temperature distribution for different height of hot heat exchanger. Height of cold heat exchanger maintained at 2 m and inlet location of hot water kept at $x_1 = 0.1\ m$

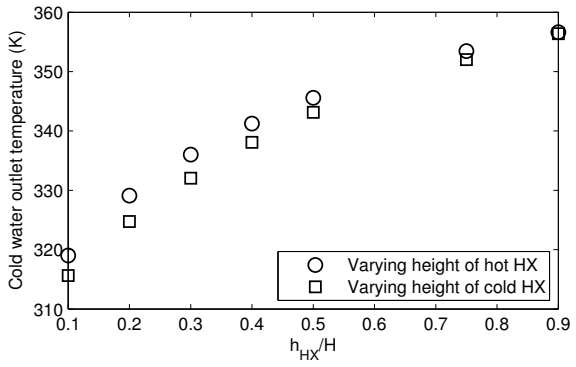

Figure 22. Effect of varying vertical length of heat exchanger on cold water outlet temperature at steady-state

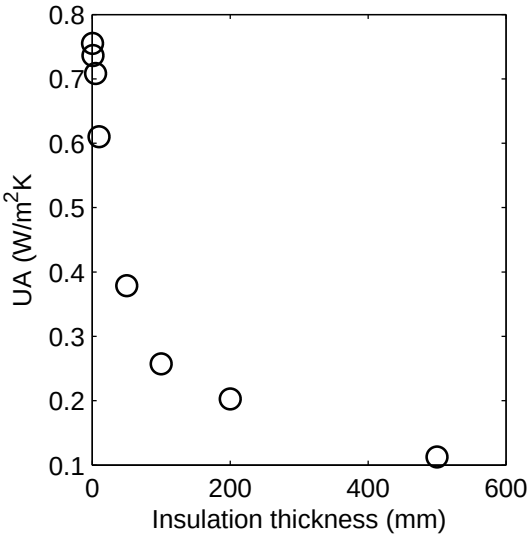

Figure 23. Heat loss coefficient vs. time for insulation thickness of 200 mm